Am J Cancer Res 2026;16(2):555-567
www.ajcr.us /ISSN:2156-6976/ajcr0171464

Original Article

GAS6 potentiates tumor progression through modulating suppressive microenvironments

Shaoteng Lu[1*], Hangxu Liu[2*], Fujie Zhang[1*], Jingyang Wang[3*], Yeting Huang[1], Jie Chen[1], Sheng Xu[1], Likun Cui[1], Tiantian Li[1]

[1]National Key Laboratory of Immunity and Inflammation, Naval Medical University/Second Military Medical University, Shanghai 200433, China; [2]The First Affiliated Hospital of Naval Medical University, Naval Medical University, 800 Xiangyin Road, Shanghai 200433, China; [3]School of Gonali Hospital Medical Technology, University of Shanghai for Science and Technology, 516 Jungong Road, Shanghai 200435, China. [*]Equal contributors.

Received January 14, 2026; Accepted February 13, 2026; Epub February 15, 2026; Published February 28, 2026

Abstract: Although growth arrest-specific 6 (GAS6), the principal ligand of the TAM receptors (TYRO3, AXL, and MERTK), acts as a central coordinator of efferocytosis, no pan-cancer analysis has been conducted. We thus first analyzed GAS6 across thirty-three tumors based on the datasets on TCGA (The Cancer Genome Atlas), TCGA-XENA (UCSC Xena), and other publicly available repositories. We observed a correlation of aberrant expression of GAS6 with malignant transformation and cancer progression, which strongly predicts worse overall survival in multiple malignancies. Transcriptomic deconvolution revealed a clear positive correlation between GAS6 levels and macrophage infiltration and polarization. Our study systematically revealed the evidence establishing GAS6 as an oncogenic driver and a regulator of the immunosuppressive microenvironment across human cancers. These findings furnish a mechanistic rationale for therapeutically targeting the GAS6/TAM axis to subvert immune tolerance and potentiate chemoradiation.

Keywords: Growth arrest-specific 6 (GAS6), tumor immune microenvironment, prognosis, pan-cancer, efferocytosis

Introduction

Despite remarkable progress in immune-checkpoint inhibitors (ICIs), key challenges-including the immunosuppressive tumor microenvironment (TME) and treatment resistance-remain unresolved and severely impede clinical outcomes [1]. A major underlying cause is the prevalent “cold tumor” phenotype within the tumor immune microenvironment (TIME), which is characterized by insufficient infiltration of effector T cells and massive accumulation of immunosuppressive cells [2, 3]. This phenotype forms an immunologically quiescent milieu that severely blunts the therapeutic potential of ICIs.

TME is recognized as a critical regulator of malignant phenotypes in tumors and consists of both normal cells and cancer cells. Macrophages are among the most abundant cell populations in the TME, known as tumor-associated macrophages (TAMs), which can regulate the proliferation, metastasis, immune response, and treatment response of tumor cells [4]. In recent years, TAMs and efferocytosis driven by these cells have been proposed as leading frontiers and focal points in tumor immunity research [5-12]. Accumulating evidence indicates that TAMs play a pivotal role in tumor immune resistance [13]. The macrophages are predominantly polarized toward an M2-like phenotype. They secrete a large number of anti-inflammatory factors while simultaneously suppressing both innate and adaptive immune responses, thereby constructing a “protective barrier” that facilitates tumor cell proliferation, invasion, and metastasis. This barrier serves as a critical driver of malignant tumor progression [14-16].

Efferocytosis serves as an essential process for maintaining tissue homeostasis under physiological conditions, efficiently eliminating apop-

https://doi.org/10.62347/JYVN8490

totic cells to prevent inflammatory. However, in the tumor microenvironment, TAMs that engulf apoptotic cells fail to elicit an immunostimulatory response [17]. Instead, they actively induce immune tolerance by secreting transforming growth factor-β (TGF-β) and recruiting regulatory T cells (Tregs) [18-21].

With respect to the human GAS6 protein, four repeated epidermal growth factor like domains (EGF1~4) and the following Gla domain (γ-carboxyglutamic acid domain) and SHBG domain (sex hormone-binding globulin domain) were identified. The GAS6-MerTK/AXL axis plays a pivotal role in bridging the upper and lower parts in the immunosuppressive cascade [12]. Phosphatidylserine (PtdSer), exposed on the surface of apoptotic cells as an "eat-me" signal, is specifically recognized and bound by GAS6. This interaction activates TAM receptors on macrophages and initiates downstream anti-inflammatory signaling pathways [17, 22-25]. Given the complex role of the GAS6 gene in tumorigenesis, it is crucial to conduct pan-cancer expression analysis and asses its associations with clinical prognosis as well as the underlying molecular mechanisms.

This study innovatively integrates multi-omics resources, including genomic, transcriptomic, proteomic, and clinical data, to systematically elucidate the expression profiles, clinical relevance, and regulatory networks of GAS6 in diverse human cancers through bioinformatic analysis and data mining. Furthermore, using both in vivo and in vitro experiments to validate its tumor-promoting mechanisms in breast cancer. These findings provide novel insights into tumor immune evasion mechanisms and inform rational combinatorial therapeutic strategies.

Materials and methods

Data sources

RNA-seq data (level-3 TPM matrices) and corresponding clinical annotations for pan-cancer were retrieved from The Cancer Genome Atlas (TCGA; https://www.cancer.gov/tcga) repository and the harmonized TCGA-XENA resource (https://xenabrowser.net). Normal-tissue controls were compiled from matched adjacent non-tumor samples in TCGA and the GTEx cohort. Genetic alteration data were acquired exclusively from mutation profiles based on TCGA datasets.

Differential expression analysis

Differential expression of GAS6 between tumor and paired normal tissues (or GTEx normal samples) for each cancer type was assessed using the Mann-Whitney U test (equivalent to the Wilcoxon rank-sum test). To ensure statistical validity, comparisons were restricted to groups meeting both "n > 3 per group" and "non-zero within-group standard deviation (SD)". Similarly, the TCGA-XENA dataset is analyzed based on the same criteria.

Survival prognosis analysis

We utilized the "Survival Map" module of GEPIA2 [26] to obtain the Overall Survival (OS) and Disease-Free Survival (DFS) significance maps data of GAS6 across all TCGA tumors. The 50% high/low expression cutoff and log-rank test were applied. Survival curves were generated via the "Survival Analysis" module.

Genetic alteration analysis

The cBioPortal (https://www.cbioportal.org/) [27, 28] was used to query the genetic alteration characteristics of GAS6 across "TCGA Pan Cancer Atlas Studies". Date on alteration frequency, mutation type, and copy number alteration (CNA) were summarized. The "Comparison" module was employed to assess survival differences between cases with or without GAS6 genetic alteration.

Immune infiltrating analysis

We used the "Immune-Gene" module of TIMER2 to explore associations between GAS6 expression and immune infiltrates. Key immune cells of interest included $CD8^+$ T cells, M2 macrophages, and Tregs. Multiple deconvolution algorithms (TIMER, CIBERSORT, XCELL, etc.) were applied, with results visualized via heatmaps and scatter plots (purity-adjusted Spearman's correlation).

GAS6-related gene enrichment analysis

To identify proteins that physically or functionally interact with GAS6, we interrogated the STRING database using high-confidence interaction thresholds (combined score ≥ 0.7) and

filtering for experimental/biochemical evidence. To identify transcriptome partners that co-vary with GAS6 across malignancies, we used the "Similar Gene Detection" module in GEPIA2, querying the entire TCGA pan-cancer expression matrix and retrieving the top 100 genes most tightly correlated with GAS6 in aggregate tumor samples.

Subsequently, gene-wise Pearson correlations with GAS6 were computed across the entire TCGA pan-cancer cohort to derive a more stringent co-expression signature. Genes showing a significant positive correlation ($r > 0.4$) and a false discovery rate (FDR)-adjusted $P < 0.05$ were retained as the "GAS6 positively-correlated gene set". Experimentally validated GAS6 interactors from STRING were intersected with this expression-correlated gene set to identify core partners (e.g., MYBBP1A) that exhibit both physical/functional binding and transcriptional co-regulation across tumors. The finalized core GAS6-associated gene list was uploaded to the DAVID (Database for Annotation, Visualization, and Integrated Discovery) and concurrently analyzed with the clusterProfiler (http://www.bioconductor.org/packages/release/bioc/html/clusterProfiler.html) R package for Kyoto encyclopedia of genes and genomes (KEGG) pathway and Gene ontology (GO) enrichment. Multiple testing correction was performed using the Benjamini-Hochberg procedure; adjusted *P* values (q values) < 0.05 were considered statistically significant.

CCK-8 assay for cell proliferation

MC38 mouse breast cancer cells were harvested by trypsinization upon reaching > 60% confluence. Following cell counting, $1\text{-}2\times10^4$ cells per well (resuspended in 200 μL RPMI-1640 medium) were seeded into a 96-well plate. Each experimental group included 3-5 technical replicates, and the assay was conducted over two consecutive days. At a designated time point each day, 10 μL of CCK-8 (Beyotime, C0038) reagent was added to each well, followed by incubation at 37°C in a humidified 5% CO_2 incubator for 2 hours. Absorbance at 450 nm was measured using a microplate reader. After measurement, plates were returned to the incubator for continued culture, and the procedure was repeated on the following day. Wells containing RPMI-1640 medium without cells served as blank controls for background subtraction. Data were analyzed statistically, and cell proliferation curves were generated.

Statistical analysis

Data are presented as mean ± SD (standard deviation) from at least three independent experiments. Statistical comparisons between two groups were performed using the unpaired, two-tailed Student's t-test for normally distributed data or the Mann-Whitney U test for non-normally distributed data. Comparisons among multiple groups were analyzed by one-way ANOVA followed by Tukey's post hoc test. Survival curves were plotted using the Kaplan-Meier method and compared by the log-rank test. The repeated measures ANOVA was employed for data collected at successive time points. Correlation analysis was assessed by Pearson's correlation coefficient. A *P* value of less than 0.05 was considered statistically significant. All statistical analyses were conducted using GraphPad Prism software (version 9.0).

Results

GAS6 gene expression in multiple cancers

In this study, we sought to evaluate the expression characteristics and clinical significance of human GAS6 across malignancies. We systematically compared GAS6 expression levels between tumor samples and corresponding normal tissues across a broad spectrum of cancers. In the TCGA dataset (**Figure 1A**), the Mann-Whitney U test revealed a pan-cancer propensity towards GAS6 upregulation. Robust overexpression ($P < 0.001$) was detected in CHOL (Cholangiocarcinoma), HNSC (Head and Neck Squamous Cell Carcinoma), and THCA (Thyroid Carcinoma). In BLCA (Bladder Urothelial Carcinoma), BRCA (Breast Carcinoma), KIRC (Kidney Renal Clear Cell Carcinoma), KIRP (Kidney Renal Papillary Cell Carcinoma), LUAD (Lung Adenocarcinoma), LUSC (Lung Squamous Cell Carcinoma), PRAD (Prostate Adenocarcinoma), and UCEC (Uterine Corpus Endometrioid Carcinoma), GAS6 exhibited a significant downregulation ($P < 0.001$). Per pre-specified QC filters, histologies

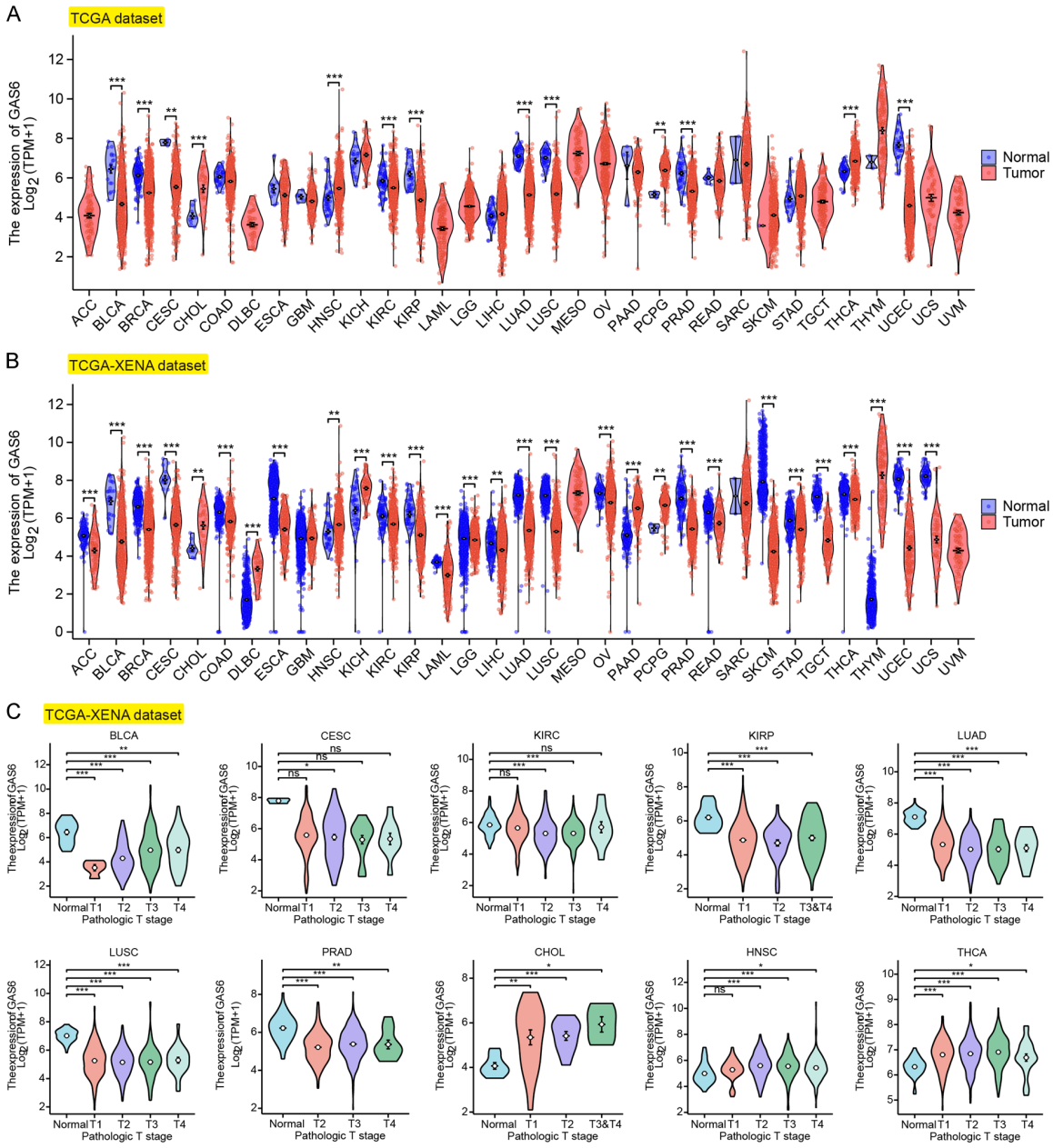

Figure 1. Expression level of the GAS6 gene in different tumors and pathological stages. A. The expression data of the GAS6 gene from the TCGA dataset in different cancer or specific cancer subtypes were analyzed through the Mann-Whitney U test. $^{**}P < 0.01$; $^{***}P < 0.001$. B. Based on the TCGA-XENE dataset, we also analyzed the expression level of the GAS6 gene between normal and tumor tissue. Statistical analyses were performed using the Mann-Whitney U test. $^{**}P < 0.01$; $^{***}P < 0.001$. C. Based on the TCGA-XENE data, the expression level of the GAS6 gene was analyzed by the main pathological T stages (T1, T2, T3, and T4) of BLCA, CESC, KIRC, KIRP, LUAD, LUSC, PRAD, CHOL, HNSC, and THCA. Statistical analyses were performed using the Kruskal-Wallis Test and Dunn's test. Differences were considered significant when $^{*}P < 0.05$.

with < 3 normal samples or zero within-group variance (SARC, SKCM, THYM, ACC, DLBC, LAML, LGG, MESO, OV) were excluded from formal statistical analysis but retained for visual inspection.

The independent, harmonized TCGA-XENA matrix (**Figure 1B**) recapitulated this expression pattern, showing significant GAS6 reduction ($P < 0.001$) in ACC (Adrenocortical Carcinoma), BLCA, BRCA, CESC (Cervical squamous cell car-

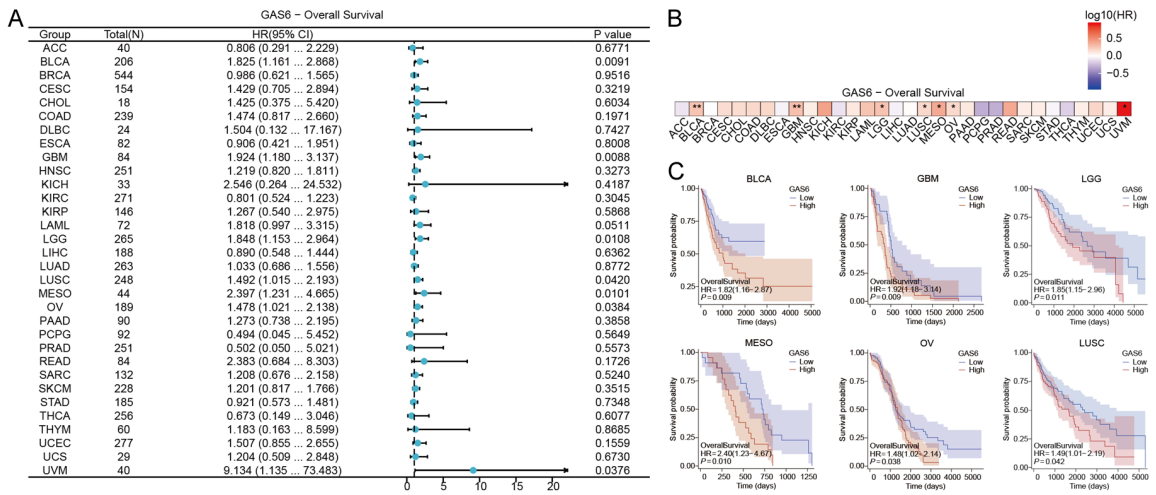

Figure 2. Correlation between GAS6 gene expression and survival prognosis of cancers in TCGA. A. A summary table of gene set enrichment analysis (GSEA) results for overall survival. B. We used the GEPIA2 tool to perform overall survival analyses of different tumors in TCGA by GAS6 gene expression. C. The survival map and Kaplan-Meier curves with positive results are given.

cinoma), COAD (Colon Adenocarcinoma), ESCA (Esophageal Carcinoma), KIRC, KIRP, PRAD, TGCT (Testicular Germ Cell Tumor), UCEC (uterine corpus endometrial carcinoma), and UCS (Uterine Carcinosarcoma), while SARC, MESO, and UVM were excluded due to insufficient sample sizes. Integrative analysis of these two independent datasets demonstrates that GAS6 expression dysregulation represents a common event in human malignancies, while the direction of its expression changes is strictly dependent on cancer type.

To figure out whether GAS6 expression is linked to local tumor progression, we stratified its abundance based on pathological T stages (T1 to T4) for each type of cancer. We used the "Pathological Stage Plot" module of GEPIA2 to observe the correlation between GAS6 expression and the pathological stages of cancers, including BLCA, CESC, KIRC, KIRP, LUAD, LUSC, PRAD, CHOL, HNSC, and THCA (**Figure 1C**).

High GAS6 correlates with increased mortality risk in various cancers

We divided the cancer cases into high-expression and low-expression groups according to the expression levels of GAS6 and investigated the correlation of GAS6 expression with the prognosis of patients with different tumors, mainly using the datasets of TCGA and GEO, respectively. In the OS analysis (**Figure 2A**, **2B**), elevated GAS6 expression emerged as an independent risk factor for poor prognosis in multiple cancers. The forest plot demonstrated significant correlations between high GAS6 expression and shortened survival in BLCA (HR = 1.82, 95% CI: 1.16-2.87, P = 0.009), GBM (HR = 1.92, 95% CI: 1.48-3.14, P = 0.009), LGG (HR = 1.85, 95% CI: 1.15-2.96, P = 0.011), LUSC (HR = 1.49, 95% CI: 1.01-2.19, P = 0.042), LUAD (HR = 1.48, 95% CI: 1.02-2.14, P = 0.038), MESO (HR = 2.40, 95% CI: 1.23-4.67, P = 0.010), OV (HR = 1.42, 95% CI: 1.02-1.97, P = 0.038), and UVM (HR = 9.13, 95% CI: 1.14-73.48, P = 0.038). Notably, UVM exhibited an exceptionally high hazard ratio (HR = 9.13). That tells us GAS6 might be playing a particularly critical role in this particular tumor type, which is rare but super aggressive (**Figure 2A**).

Our meta-analysis data further confirmed the correlation between GAS6 expression and prognosis for MESO, LUSC, LGG, GBM, and BLCA, demonstrating significant survival disparities between high and low GAS6 expression groups (**Figure 2C**). High GAS6 expression was similarly associated with accelerated disease progression across various cancers, further confirming that elevated GAS6 expression increases mortality risk.

GAS6 expression can predict cancer prognosis

We used the timeROC package to quantify the predictive power of GAS6 expression for 1-year survival across 20 cancer types. The area

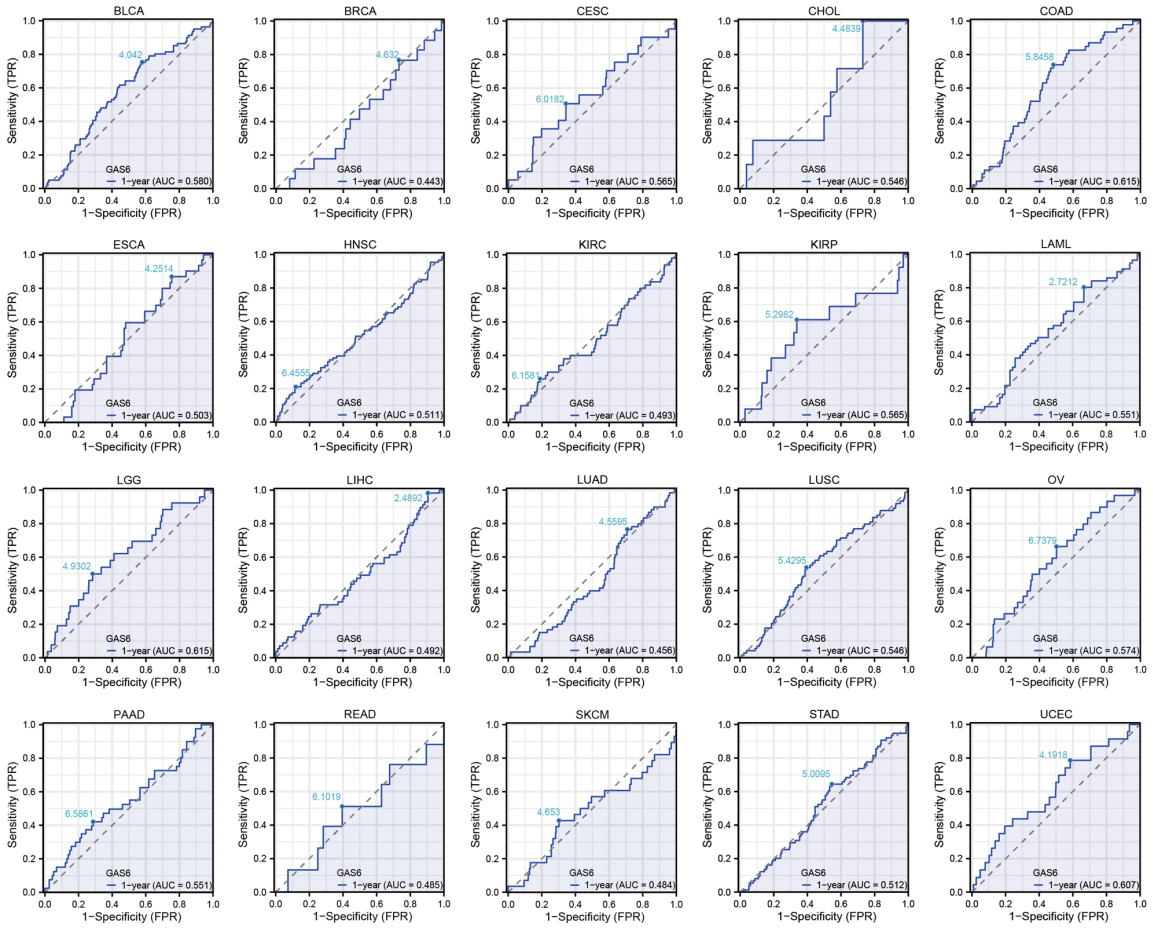

Figure 3. Prognostic performance of GAS6 expression for 1-year survival across multiple cancer types. AUC > 0.5: High GAS6 expression was correlated with poor 1-year survival (serving as a risk factor). AUC values ranging from 0.44 to 0.62: GAS6 had limited predictive capacity as an independent 1-year prognostic biomarker.

under the curve (AUC) values revealed striking tumor-type specificity. High GAS6 transcript level correlated with poor 1-year survival outcomes in BLCA (AUC = 0.580), COAD (AUC = 0.615), and LGG (AUC = 0.615). All of these AUC had values above 0.5. In contrast, GAS6 actually showed a protective tendency in BRCA (AUC = 0.443) and LUAD (AUC = 0.456), in which increased expression was associated with better 1-year survival (AUC < 0.5) (**Figure 3**). As for the remaining cancer types, AUC values clustered around 0.5, indicating limited ability to discriminate short-term prognosis.

All these data indicate that elevated GAS6 expression demonstrates consistent prognostic value across multiple cancer types, with particularly prominent associations observed in LGG/GBM, OV, PAAD, and COAD/READ. In these malignancies, high GAS6 expression correlates with increased overall mortality risk.

Genetic alteration of GAS6 associates with tumor progression

We examined the genetic alteration status of GAS6 across tumor samples in TCGA cohorts. As shown in **Figure 4A**, UCEC exhibited the highest frequency of GAS6 genetic alteration (> 6%), with mutations being the predominant alteration type. In Sarcoma samples, the major type of copy number alteration (CNA) was amplification, with an overall genetic alteration frequency reaching approximately 4% (**Figure 4A**). The types, sites, and case number of the GAS6 genetic alteration are further presented in **Figure 4B**. We found that a missense mutation represented a major type of genetic alteration in GAS6. Specific alterations, including G150Afs*49, R151Pfs*27 and V673Wfs*85/Rfs*37, induce frameshift mutations of the GAS6 gene, translation from G (Glycine) to A (Alanine) at the 150 site of GAS6 protein, R

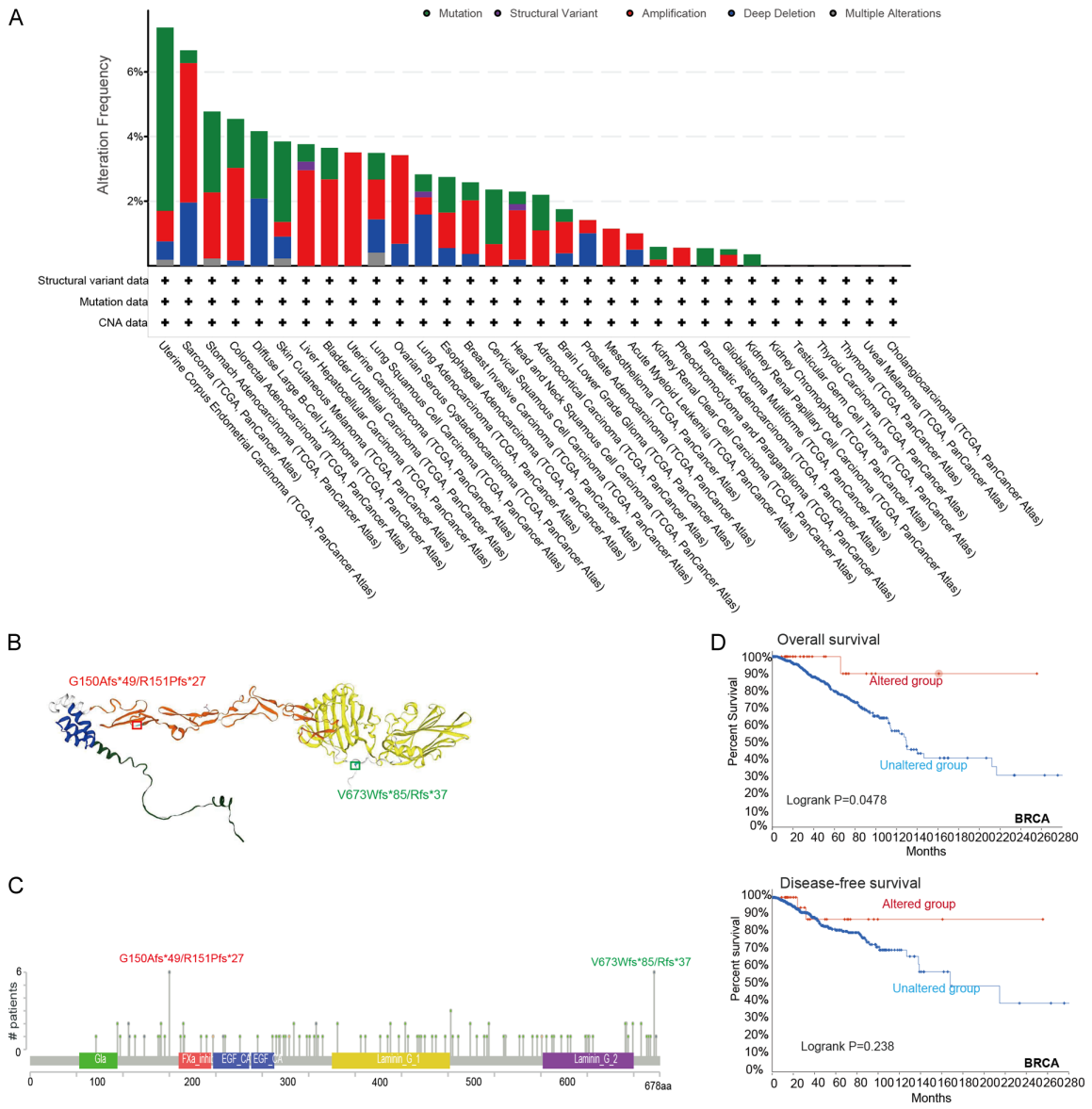

Figure 4. Mutation feature of GAS6 in different tumors of TCGA. We analyzed the mutation features of GAS6 for the TCGA tumors using the cBioPortal tool. A. The alteration frequency with the mutation type. B. The highest alteration frequency (G150Afs*49, R151Pfs*27 and V673Wfs*85/Rfs*37) in 3D structure of GAS6. C. The alteration frequency with mutation site. D. We also analyzed the potential correlation between mutation status and overall and disease-free survival of GAS6 using the cBioPortal tool.

(Arginine) to P (Proline) at 151 site of GAS6 protein, and V (Valine) to W (Tryptophan) or R (Arginine) at 673 site of GAS6 protein. We can observe these three sites in the 3D structure of GAS6 protein (**Figure 4C**). Additionally, we explored the potential association between genetic alteration of GAS6 and the clinical survival prognosis of cases with different types of cancer. The data of **Figure 4D** indicate that BRCA cases with altered GAS6 showed better prognosis in overall (P = 0.0478) survival, but not disease-free (P = 0.238) survival, compared with cases without GAS6 alteration, which deserves more in-depth research.

GAS6 expression associates with immune infiltration

The TIME exerts a profound impact on the efficacy of immunotherapy [29, 30]. By conferring an immunosuppressive phenotype, malignant cells are able to evade immune surveillance,

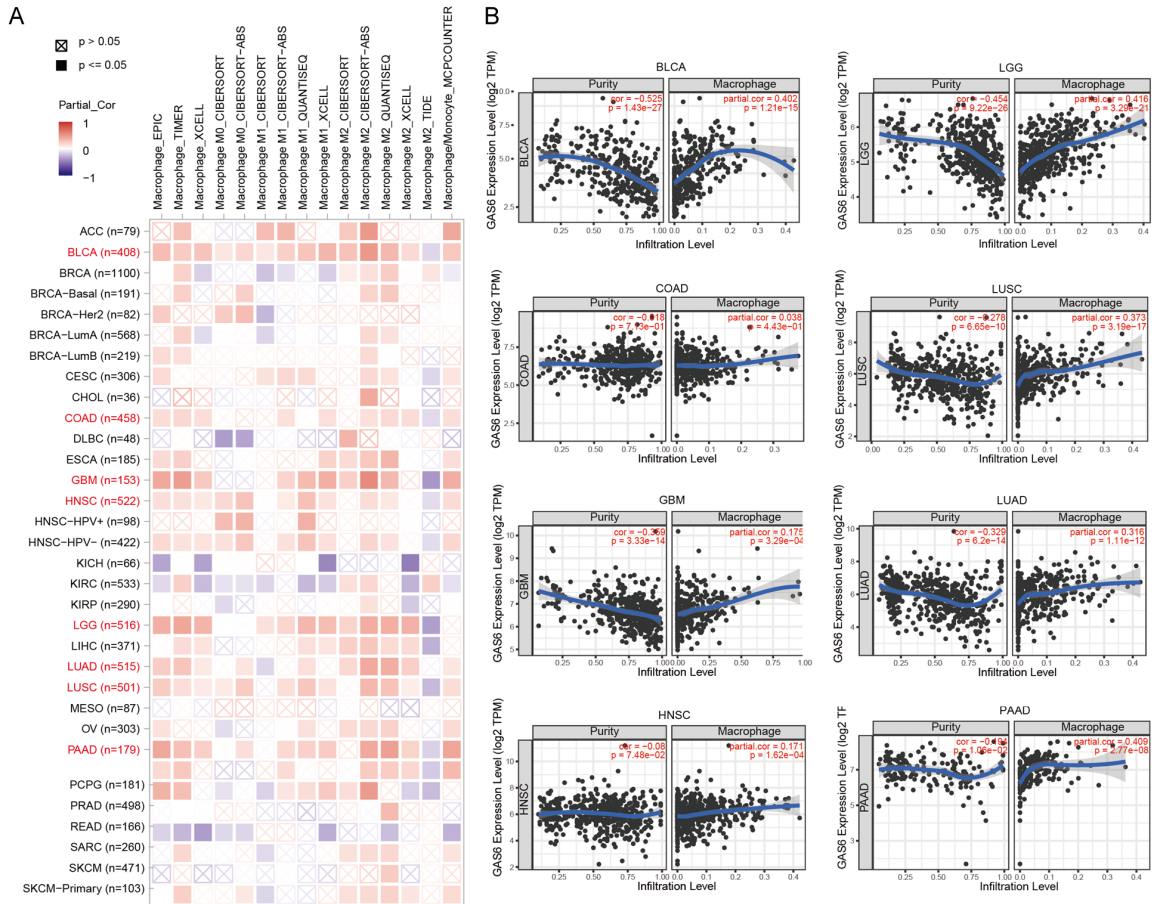

Figure 5. Correlation analysis between GAS6 expression and immune infiltration of tumor-associated macrophages. Different algorithms were used to explore the potential correlation between the expression level of the GAS6 gene and infiltration levels of tumor-associated macrophages across all types of cancer in TCGA.

facilitating cancer initiation, progression, recurrence, metastasis, and ultimately treatment resistance [31]. In the current study, we took a systematically approach to explore the potential association between the infiltration levels of various immune cell subsets and GAS6 gene expression across different cancer types in the TCGA database by employing algorithms including EPIC, TIMER, XCELL, CIBERSORT, CIBERSORT-ABS, MCPCOUNTER, and TIDE.

We found that the correlation patterns between GAS6 and immune cell infiltration varied across different cancer types. The correlations between GAS6 and multiple immune cell subsets were generally strong in KIRC, LUAD, and PAAD, whereas such correlations were overall weak in THCA and PRAD (Figure S1). Through a series of analyses, we found that GAS6 expression was significantly positively correlated with the infiltration levels of macrophages, monocytes, neutrophils, and cancer-associated fibroblasts (CAFs) in multiple cancer types (**Figures 5A** and S1). The positive correlation between GAS6 and CAFs was most prominent in KIRC, LUAD and PAAD (Figure S1). In contrast, GAS6 expression exhibited a negative or no significant correlation with the infiltration levels of $CD8^+$ T cells, cytotoxic lymphocytes and natural killer (NK) cells in most cancer types.

Additionally, the immune infiltration levels of various macrophage subsets were statistically significantly positively correlated with GAS6 expression in BLCA, GBM, LGG, LUAD, LUSC, PAAD, and HNSC (**Figure 5A**). Accumulating evidence has indicated that TAMs within the

tumor microenvironment are involved in the regulation of tumor immunity [32]. This result was consistent across all or most of the aforementioned algorithms. **Figure 5B** presents the scatter plot data of the abovementioned cancers generated by the EPIC algorithm. Most significantly, GAS6 expression levels were significantly positively correlated with TAM infiltration levels in LGG (**Figure 5B**, r = 0.416, *P* = 3.29e-21).

Enrichment analysis of GAS6-related partners

To further explore the molecular mechanism of GAS6 in tumorigenesis, we perform pathway enrichment analyses based on both its physical interactors and the genes. We used the STRING database to obtain 20 proteins that interact with GAS6 (**Figure 6A**). We investigated whether the functional network of GAS6 is specific to different cancer types, which would help us to uncover common and unique mechanisms behind its role in promoting tumors. The genes co-expressed with GAS6 were primarily enriched in intracellular transport, metabolism, and basic signaling pathways in COAD. KEGG enrichment analysis revealed significant enrichment in endocytosis, mTOR signaling, and insulin signaling pathway (**Figure 6B**). The GO enrichment analysis data indicated these genes were concentrated in GTPase binding and regulatory activities at the molecular function level (**Figure 6C**). In striking contrast, in LUSC, genes co-expressed with GAS6 showed a totally different functional tendency, being highly concentrated in extracellular matrix (ECM) and cell adhesion-related pathways (**Figure 6E**). For KEGG enrichment analysis in LUSC, the most significantly enriched pathways were focal adhesion, cell adhesion molecules, and ECM-receptor interaction (**Figure 6D**).

To investigate the potential common regulatory mechanisms of GAS6 across different cancer types, we performed GAS6-centered co-expression analysis in COAD and LUSC. We used transcriptomic data from the TCGA database and integrated high-confidence protein-to-protein interactions from the STRING database. As shown in **Figure 6F**, in COAD, intersecting 7,306 genes significantly co-expressed with GAS6 with 58 experimentally validated GAS6 interactors yielded 34 high-confidence candidate genes. In LUSC, the overlap between 1,356 co-expressed genes and the same interactor set resulted in 7 candidates. TGFβ1 was the only common interactor identified in COAD and LUSC, suggesting a conserved partnership with GAS6. Spearman correlation analysis confirmed this association, showing significant positive correlations between GAS6 and TGFβ1 transcript levels in both COAD (R = 0.246, *P* < 0.001) (**Figure 6G**) and LUSC (R = 0.289, *P* < 0.001) (**Figure 6H**), supporting the reliability of our bioinformatic predictions. Spearman correlation analysis in BRCA similarly validated a positive correlation between GAS6 and TGFβ1 transcript levels (R = 0.588, *P* < 0.001).

GAS6-associated immunosuppression fuels MC38 tumor progression

To confirm the pro-tumorigenic function of GAS6 predicted by our bioinformatic analysis, we conducted functional studies in the MC38 colon cancer model. In vitro assays showed that GAS6 had no noticeable effect on the short-term proliferation of MC38 cells (**Figure 7A**). Given that GAS6 is known to regulate efferocytosis and macrophage polarization, we investigated its impact on the phenotypic of macrophages following coculture with tumor cells. For this purpose, we assayed TGFβ1 and CD206 mRNA levels as the marker of resolution. We found that the protein and mRNA levels of TGFβ1 were higher in bone marrow-derived macrophages (BMDMs) co-cultured with GAS6-overexpressing MC38 tumor cell (**Figure 7B**, **7C**), which is consistent with our earlier bioinformatics findings. CD206 mRNA level in GAS6-OE group was also higher than shGAS6 group and CTR group (**Figure 7D**). In vivo experiments demonstrated that compared with the wild-type control group (MC38-WT), subcutaneous tumor growth was significantly inhibited in the GAS6 knockout group (MC38-GAS6-KO) (**Figure 7E**, **7F**). This suggests that the impact of GAS6 on tumor growth depends on the tumor microenvironment. Immunohistochemical analysis of MC38 tumors revealed that the rate of F4/80-positive cells was higher in the GAS6-KO group than the WT group (**Figure 7G**). In contrast, CD206 positive cells were reduced in the GAS6-KO group (**Figure 7G**). Thus, the knockout of GAS6 promotes macrophage infiltration, especially M1-type macrophages. In summary, the in vitro and in

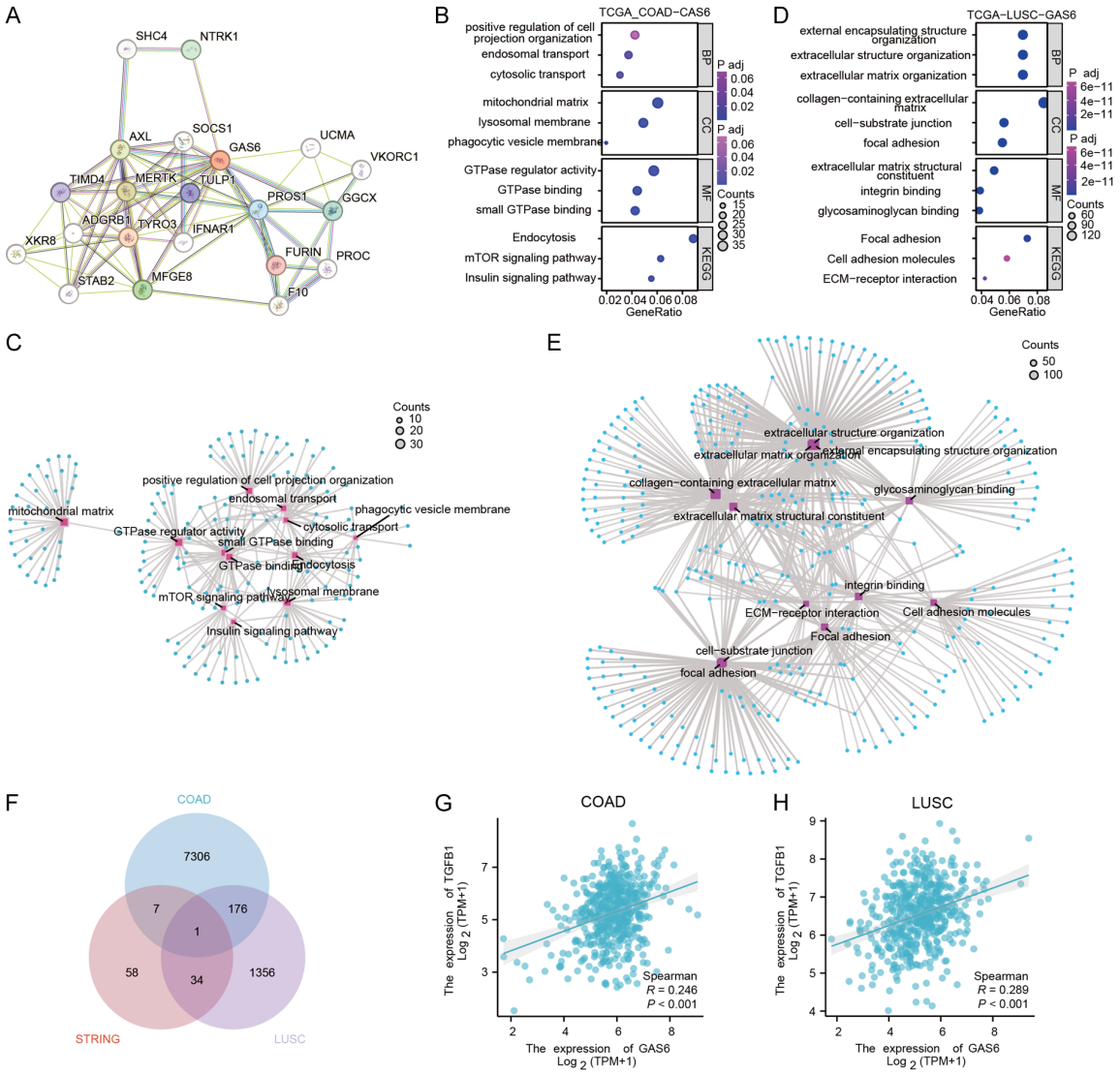

Figure 6. GAS6-related gene enrichment analysis. A. We first obtained the available experimentally determined GAS6-binding proteins using the STRING tool. B. Based on the GAS6-binding and interacting genes, KEGG pathway analysis in COAD was performed. C. The cnetplot for the molecular function data in GO analysis for COAD is also shown. D. KEGG pathway analysis in LUSC was performed. E. The cnetplot for the molecular function data in GO analysis for LUSC is also shown. F. An intersection analysis was performed on GAS6-binding genes and their correlated genes in both COAD and LUSC. G. Expression Correlation between GAS6 and TGFβ1 in COAD with Statistical Significance Assessed by Spearman Correlation Analysis. H. Expression Correlation between GAS6 and TGFβ1 in LUSC with Statistical Significance Assessed by Spearman Correlation Analysis.

vivo results directly confirm the critical role of GAS6 in promoting colon cancer tumor growth.

Discussion

Previous reports have reported that GAS6 and its cognate TAM receptors acts on tumor immune evasion mainly through the regulation of efferocytosis and the establishment of an immunosuppressive tumor microenvironment [17, 23, 25, 33]. In this study, we further consolidated the role of GAS6 in mediating tumor immune evasion through a comprehensive pan-cancer analysis [34-37]. We further found that elevated GAS6 expression in tumor tissues correlates with markedly reduced infiltration of immune cells, most prominently macrophages. This alteration permits tumors to construct an immunosuppressive barrier that fosters malignant progression.

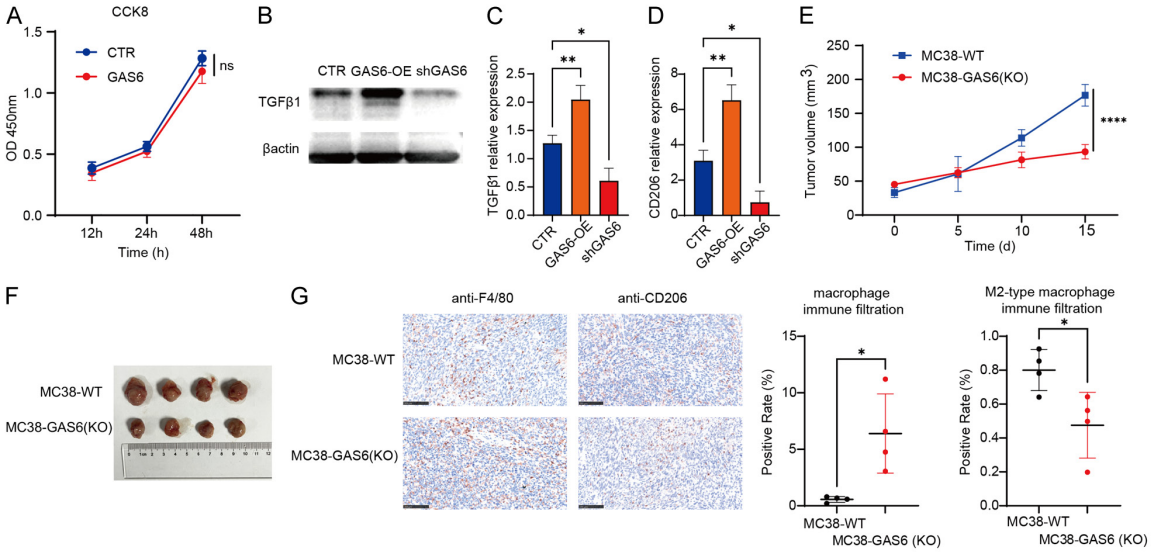

Figure 7. GAS6 promotes tumor growth in vivo. A. CCK-8 assay showing cell viability of wild-type (WT), GAS6-overexpressing (GAS6) (n = 5 biological replicates/group). Data are presented as mean ± SD. B. Western Blot analysis of TGFβ1 protein expression in BMDM cocultured with WT, GAS6-OE, or shGAS6 MC38 tumor (n = 3 samples/group). C, D. Quantitative analysis of TGFβ1 and CD206 mRNA expression level in (B). E. Tumor growth curves of mice bearing MC38-WT or MC38-GAS6 knockout (KO) tumors over 15 days (n = 4 samples/group). F. Representative photographs of tumors excised from mice injected with MC38-WT or MC38-GAS6 (KO) cells (n = 4 samples/group). G. Representative immunohistochemical images showing the expression and distribution of F4/80 and CD206 in subcutaneous tumor tissues from MC38-WT and MC38-GAS6-KO groups (n = 4 samples/group). Scale bar: 100 μm. All mRNA data are expressed relative to the indicated control groups. Data are mean ± SD. Data from continuous time points was analyzed by the repeated measures ANOVA. Significance was determined by two-tailed Student's t-test or one-way ANOVA with Tukey's post hoc analysis. "ns" means $P > 0.05$, "*" means $P < 0.05$, "**" means $P < 0.01$, "***" means $P < 0.001$, "****" means $P < 0.0001$.

In this work, we used the GEPI2 tool to detect a statistical correlation between the expression of GAS6 and tumor progression. GAS6 expression was significantly upregulated in multiple cancer types, including CHOL, HNSC, and THCA, but showed no strong pan-cancer consistency. Survival analysis further indicated that high GAS6 expression is associated with poor prognosis in patients with BLCA, GBM, LGG, LUSC, LUAD, MESO, OV, and UVM. Among these, UVM showed a particularly high hazard ratio (HR = 9.13).

In terms of immune correlation, GAS6 expression positively correlates with macrophage infiltration. This association is especially prominent in M2-polarized macrophage subsets in BLCA, GBM, LGG, LUAD, LUSC, PAAD, and HNSC. Functional enrichment analysis revealed that high GAS6 activity is closely linked to efferocytosis, TAM receptor signaling, and inflammatory resolution.

In vivo experiments demonstrated that GAS6 knockout significantly suppresses the growth of MC38 colon cancer xenografts. In contrast, GAS6 showed no direct effect on tumor cell proliferation in vitro. This discrepancy highlights the central role of TME in mediating the oncogenic functions of GAS6. Moreover, experiments validated the positive correlation between high GAS6 expression and TGFβ1 expression of macrophages, as suggested by bioinformatics analysis. GAS6 overexpression not only elevates TGFβ1 levels but also specifically recruits M2-type macrophages. The underlying molecular mechanisms by which GAS6 regulates TGFβ1 expression require further investigation.

Notably, GAS6 expression is significantly downregulated in BLCA, KIRP, LUAD, and PRAD. In BRCA and LUAD, high GAS6 expression correlates with improved 1-year patient survival, suggesting a potential tumor-suppressive role in specific contexts. Thus, GAS6 is not simply an oncogene but rather a finely tuned modulator in tumor biology.

Taken together, our first pan-cancer analyses of GAS6 confirms that it is a critical regulator of tumor progression, primarily through shaping

an immunosuppressive tumor microenvironment. Future investigations should clarify the molecular mechanisms underlying its context-dependent functions, which will provide guidance for developing targeted therapies such as TAM receptor inhibitors.

Acknowledgements

This work was supported by the National Natural Science Foundation of China (82371782) and the Yizhang Talent Development Fund of Naval Medical University (JCYZRC-D-033).

Disclosure of conflict of interest

None.

Address correspondence to: Sheng Xu, Likun Cui and Tiantian Li, National Key Laboratory of Immunity and Inflammation, Naval Medical University/Second Military Medical University, Shanghai 200433, China. E-mail: xusheng@immunol.org (SX); POPPY199609@163.com (LKC); tian.tian.li@outlook.com (TTL)

References

[1] Pail O, Lin MJ, Anagnostou T, Brown BD and Brody JD. Cancer vaccines and the future of immunotherapy. Lancet 2025; 406: 189-202.
[2] Feng Y, Yang H, Liang G, Chen J, Li T, Wang Y, Chang J, Li Y, Yang M, Zhou X, Wang Z and Ge C. Immune checkpoint inhibitors combined with oncolytic virotherapy: synergy, heterogeneity, and safety in cancer treatment. Oncol Res 2025; 33: 3801-3836.
[3] Varsanyi C and Birge RB. Mertk signaling and immune regulation in T cells. J Leukoc Biol 2024; 117: qiae253.
[4] Zhang T, Zhao X, Gao T and Ma F. Tumor-associated macrophages in hepatocellular carcinoma: cellular plasticity and therapy resistance in crosstalk. J Pharm Anal 2026; 16: 101384.
[5] Zhang H, Diao QF, Yang CB, Li JW, Wu XL and Xiao CG. Roles of tumor-associated macrophages in the development of colorectal cancer and their potential as therapeutic targets. Zhongguo Yi Xue Ke Xue Yuan Xue Bao 2025; 47: 1026-1036.
[6] Wang L, Chu H, Chen D, Wei Y, Jia J, Li L, He L, Peng L, Liu F, Huang S, Jin Z, Zhou D, Fang W, Jiang T, Xu S, Ding X, Cai H, Liu X, Jia Q, Zhu B and Chu Q. SLC2A1(+) tumour-associated macrophages spatially control CD8(+) T cell function and drive resistance to immunotherapy in non-small-cell lung cancer. Nat Cell Biol 2026; 28: 338-348.
[7] Zhang Y, Zang H and Wen Q. Macrophage polarization in tumors: the impact of efferocytosis. Int Immunopharmacol 2026; 168: 115807.
[8] Huang P, Liu Y, Zhao C, Wang C, Wang L, Luo M, Wang W, Shan W, Liu X, Li B, Wang Z, Deng H and Chen X. Permanent efferocytosis prevention by terminating mertk recycle on tumor-associated macrophages for cancer immunotherapy. J Am Chem Soc 2025; 147: 15901-15914.
[9] Lecoultre M, Chliate S, Espinoza FI, Tankov S, Dutoit V and Walker PR. Radio-chemotherapy of glioblastoma cells promotes phagocytosis by macrophages in vitro. Radiother Oncol 2024; 190: 110049.
[10] Pop OT, Geng A, Flint E, Singanayagam A, Ercan C, Possamai L, Patel VC, Kuenzler P, Meier MA, Soysal S, Hruz P, Kollmar O, Tatham KC, Ward JK, Müllhaupt B, Weber A, Wendon J, Niess JH, Heim M, Semela D, Weston C, Antoniades CG, Terracciano LM, Triantafyllou E, Brenig RG and Bernsmeier C. AXL expression on homeostatic resident liver macrophages is reduced in cirrhosis following GAS6 production by hepatic stellate cells. Cell Mol Gastroenterol Hepatol 2023; 16: 17-37.
[11] Huang H, Jiang J, Chen R, Lin Y, Chen H and Ling Q. The role of macrophage TAM receptor family in the acute-to-chronic progression of liver disease: from friend to foe? Liver Int 2022; 42: 2620-2631.
[12] Lahey KC, Gadiyar V, Hill A, Desind S, Wang Z, Davra V, Patel R, Zaman A, Calianese D and Birge RB. Mertk: an emerging target in cancer biology and immuno-oncology. Int Rev Cell Mol Biol 2022; 368: 35-59.
[13] Christofides A, Strauss L, Yeo A, Cao C, Charest A and Boussiotis VA. The complex role of tumor-infiltrating macrophages. Nat Immunol 2022; 23: 1148-1156.
[14] Li Y and Wang L. Bidirectional regulation in the tumour microenvironment: the interaction between tumour-associated macrophages and t cells reshapes the paradigm of cancer immunotherapy. Immunology 2026; [Epub ahead of print].
[15] Yang Q, Yan J and Yang Q. Metabolic reprogramming of efferocytosis in the tumour microenvironment: from apoptotic-cell clearance to therapeutic targeting. Clin Transl Med 2026; 16: e70601.
[16] Hu S, Heng H, Yang F, Wang M, Liu G, Xiang Y and Miao H. The metabolism-immune axis in colorectal cancer: remodeling the tumor microenvironment through metabolite signaling. Front Immunol 2025; 16: 1735873.
[17] Tokarska-Domżałowicz W and Zdżalik-Bielecka D. At the intersection of immunology and oncology: TAM receptors in the regulation of im-

mune responses and tumorigenesis-related processes. Postepy Biochem 2025; 71: 238-251.
[18] Bosurgi L, Cao YG, Cabeza-Cabrerizo M, Tucci A, Hughes LD, Kong Y, Weinstein JS, Licona-Limon P, Schmid ET, Pelorosso F, Gagliani N, Craft JE, Flavell RA, Ghosh S and Rothlin CV. Macrophage function in tissue repair and remodeling requires IL-4 or IL-13 with apoptotic cells. Science 2017; 356: 1072-1076.
[19] Schilperoort M, Ngai D, Sukka SR, Avrampou K, Shi H and Tabas I. The role of efferocytosis-fueled macrophage metabolism in the resolution of inflammation. Immunol Rev 2023; 319: 65-80.
[20] Li Y, Li P, Song J, Zhang X, Xiao H, Wang R, Duan Z, Luo K and Xu X. Targeting efferocytosis for tissue regeneration: from microenvironment reprogramming to clinical translation. Theranostics 2026; 16: 3697-3734.
[21] Tajbakhsh A, Gheibi Hayat SM, Movahedpour A, Savardashtaki A, Loveless R, Barreto GE, Teng Y and Sahebkar A. The complex roles of efferocytosis in cancer development, metastasis, and treatment. Biomed Pharmacother 2021; 140: 111776.
[22] Lemke G. Biology of the TAM receptors. Cold Spring Harb Perspect Biol 2013; 5: a009076.
[23] Lew ED, Oh J, Burrola PG, Lax I, Zagórska A, Través PG, Schlessinger J and Lemke G. Differential TAM receptor-ligand-phospholipid interactions delimit differential TAM bioactivities. Elife 2014; 3: e03385.
[24] Rothlin CV, Ghosh S, Zuniga EI, Oldstone MB and Lemke G. TAM receptors are pleiotropic inhibitors of the innate immune response. Cell 2007; 131: 1124-1136.
[25] Graham DK, DeRyckere D, Davies KD and Earp HS. The TAM family: phosphatidylserine sensing receptor tyrosine kinases gone awry in cancer. Nat Rev Cancer 2014; 14: 769-785.
[26] Tang Z, Kang B, Li C, Chen T and Zhang Z. GEPIA2: an enhanced web server for large-scale expression profiling and interactive analysis. Nucleic Acids Res 2019; 47: W556-W560.
[27] Gao J, Aksoy BA, Dogrusoz U, Dresdner G, Gross B, Sumer SO, Sun Y, Jacobsen A, Sinha R, Larsson E, Cerami E, Sander C and Schultz N. Integrative analysis of complex cancer genomics and clinical profiles using the cBioPortal. Sci Signal 2013; 6: pl1.
[28] Cerami E, Gao J, Dogrusoz U, Gross BE, Sumer SO, Aksoy BA, Jacobsen A, Byrne CJ, Heuer ML, Larsson E, Antipin Y, Reva B, Goldberg AP, Sander C and Schultz N. The cBio cancer genomics portal: an open platform for exploring multidimensional cancer genomics data. Cancer Discov 2012; 2: 401-404.
[29] Meyiah A, Khan FI, Alfaki DA, Murshed K, Raza A and Elkord E. The colorectal cancer microenvironment: preclinical progress in identifying targets for cancer therapy. Transl Oncol 2025; 53: 102307.
[30] Lei X, Lei Y, Li JK, Du WX, Li RG, Yang J, Li J, Li F and Tan HB. Immune cells within the tumor microenvironment: biological functions and roles in cancer immunotherapy. Cancer Lett 2020; 470: 126-133.
[31] Chu X, Li X, Zhang Y, Dang G, Miao Y, Xu W, Wang J, Zhang Z and Cheng S. Integrative single-cell analysis of human colorectal cancer reveals patient stratification with distinct immune evasion mechanisms. Nat Cancer 2024; 5: 1409-1426.
[32] Myers KV, Amend SR and Pienta KJ. Targeting Tyro3, Axl and MerTK (TAM receptors): implications for macrophages in the tumor microenvironment. Mol Cancer 2019; 18: 94.
[33] Dave F, Herrera K, Lockley A, van de Weijer LL, Henderson S, Sofela AA, Hook L, Adams CL, Ercolano E, Hilton DA, Maze EA, Kurian KM, Ammoun S and Hanemann CO. Targeting MERTK on tumour cells and macrophages: a potential intervention for sporadic and NF2-related meningioma and schwannoma tumours. Oncogene 2024; 43: 3049-3061.
[34] Purohit S, Mandal G, Biswas S, Dalui S, Gupta A, Chowdhury SR and Bhattacharyya A. AXL/GAS6 signaling governs differentiation of tumor-associated macrophages in breast cancer. Exp Cell Res 2025; 444: 114324.
[35] Kim TH, Lee D, Oh HJ, Ham IH, Lee DM, Lee Y, Zhang Z, Ke D and Hur H. Targeting GAS6/AXL signaling improves the response to immunotherapy by restoring the anti-immunogenic tumor microenvironment in gastric cancer. Life Sci 2023; 335: 122230.
[36] Dai JC, Yang JY, Chang RQ, Liang Y, Hu XY, Li H, You S, He F and Hu LN. GAS6-mediated dialogue between decidual stromal cells and macrophages is essential for early pregnancy maintenance by inducing M2-like polarization and cell proliferation of decidual macrophages. Mol Hum Reprod 2022; 28: gaac006.
[37] Tanaka M and Siemann DW. Gas6/Axl signaling pathway in the tumor immune microenvironment. Cancers (Basel) 2020; 12: 1850.

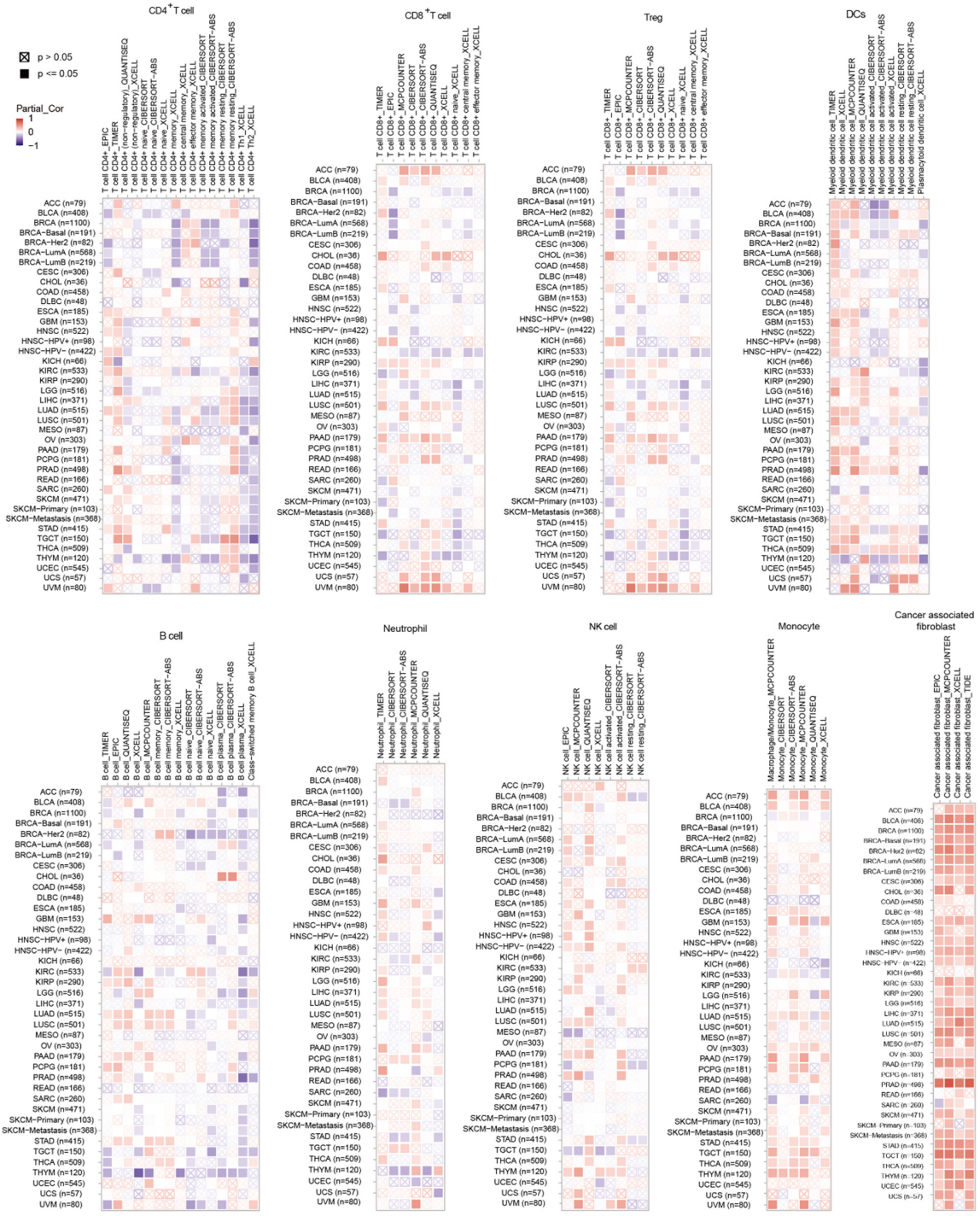

Figure S1. Correlation analysis between GAS6 expression and infiltrating immune cells across all types of cancer in TCGA. The heatmap displays the correlation distribution of $CD4^+$ T cells, $CD8^+$ T cells, Tregs, dendritic cells (DCs), B cells, neutrophils, NK cells, monocytes, and cancer-associated fibroblasts across all types of TCGA cancer. These correlations were evaluated using analytical methods such as EPIC, CIBERSORT, and XCELL. The color scale ranges from -1 to 1, with blue indicating negative correlation and red indicating positive correlation.